CFD Modeling of LPG Vessels Under Fire Exposure Conditions

Arianna D'Aulisa, Alessandro Tugnoli, and Valerio Cozzani
LISES, Dipt. di Ingegneria Civile, Chimica, Ambientale e dei Materiali, Alma Mater Studiorum - Università di Bologna, via Terracini n.28, 40131 Bologna, Italy

Gabriele Landucci
Dipt. di Ingegneria Civile e Industriale, Università di Pisa, Largo Lucio Lazzarino, 56126 Pisa, Italy

Albrecht Michael Birk
Dept. of Mechanical and Materials Engineering, McLaughlin Hall, Queen's University, Kingston, ON, Canada K7L 3N6

DOI 10.1002/aic.14599
Published online September 2, 2014 in Wiley Online Library (wileyonlinelibrary.com)

Fire exposure of tanks used for the storage and transportation of liquefied gases under pressure may cause complex heat- and mass-transfer phenomena that may contribute to compromise the integrity of the vessels in accident scenarios. Heat transfer through vessel lading results in the heat-up of the internal fluid and the increase of vessel internal pressure. However, local temperature gradients in the liquid phase cause liquid stratification phenomena that result in a more rapid vaporization and pressure build-up in the liquid phase. These fundamental phenomena were analyzed by a computational fluid dynamic model. The model was specifically focused on the early steps of vessel heat-up, when liquid stratification plays a relevant role in determining the vessel internal pressure. A two-dimensional transient simulation was set up using ANSYS FLUENT in order to predict the evolution of the liquid and vapor phases during the tank heat up. The model was validated against large scale experimental data available for liquefied petroleum gas vessels exposed to hydrocarbon fires, and was applied to case studies derived from recent accidental events in order to assess the expected time of pressure build-up in different fire scenarios. © 2014 American Institute of Chemical Engineers *AIChE J*, 60: 4292–4305, 2014

Keywords: heat transfer, liquid stratification, computational fluid dynamics, safety, loss prevention, major accident hazard

Introduction

Transportation of liquefied flammable products (such as liquefied petroleum gas - LPG, propylene, butadiene, etc., but also unstabilized crude oil) has a strategic importance for the economy of industrialized countries. Nevertheless, road and rail transportation of such hazardous materials is affected by severe accidents.[1,2] Some occurred also recently in North America (Lac Megantic, Canada,[3] and Casselton, ND[4] in 2013) and in Europe (Viareggio, Italy[5,6] in 2009), raising public concerns on the safety of such activities.

Past accident data analysis[7] shows that about 33% of accidents occurred during road or rail LPG transportation resulted in boiling liquid expanding vapor explosions (BLEVEs) and associated fireballs[8–11] induced by fire exposure (hot BLEVEs).[10,11] The occurrence of a hot BLEVE and its possible prevention is highly influenced by the internal pressure build-up in the vessel exposed to fire, that in turn depends on liquid temperature. In available large-scale experimental tests, nonuniform temperature distributions were shown to appear, generating liquid stratification and strongly influencing the internal pressure of the vessel, thus affecting time to failure and time available for successful accident mitigation.[11–13]

Several studies afford the general theme of heat-induced liquid stratification. Recent publications showed the results obtained modeling thermal stratification in systems in which water is used, such as electronics and photovoltaic cooling equipment, thermosiphon and hydrosiphon heat exchangers, solar-thermal heat absorbers, and passive decay heat removal systems.[14,15] Thermal stratification may also affect nuclear reactors water cooling systems[16] and cryogenic storage systems.[17,18] Recent studies showed the potentialities of distributed parameters code in simulating liquid hydrogen and liquefied natural gas stratification and destratification phenomena.[19–22]

Systems containing LPG exposed to heat flows typical of industrial fires feature relevant specific aspects due to physical properties of the substances and to the heat flows applied. To date mostly simplified lumped parameters models were developed to assess LPG stratification,[12,23–28] that assume liquid and vapor as homogenous phases. Aydemir et al.[29] showed an example of lumped approach for modeling the liquid stratification under fire exposure in the code "PLGS-I." The lumped approach consisted in dividing the liquid space of the fired vessel in two major control

Correspondence concerning this article should be addressed to V. Cozzani at valerio.cozzani@unibo.it.

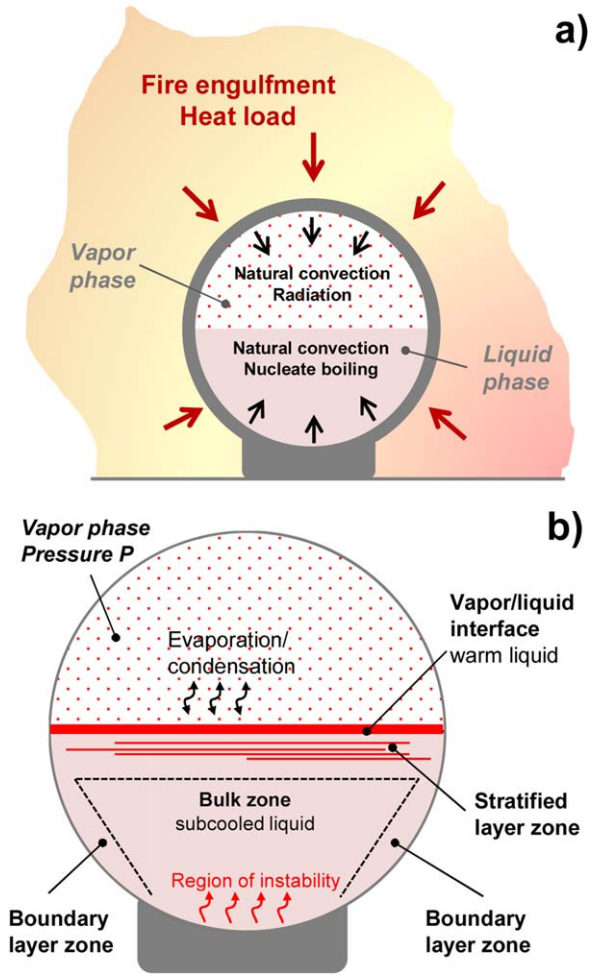

Figure 1. (a) Physical phenomena involved in vessel heat-up; (b) schematization of thermal stratification phenomenon (Adapted from Ref. 35).

[Color figure can be viewed in the online issue, which is available at wileyonlinelibrary.com.]

volumes, linked by the evaporation of a stratified interface, in which the energy balance was solved. Similar lumped approaches were also shown by Birk[30] and Dancer and Sallet,[31] respectively, for the codes "TANKCAR" and "TAC7," in which the lading was subdivided in several zones. A simplified approach to the assessment of stratification was more recently proposed by Gong et al.[32] showing sufficient agreement with small scale experimental results; this model was also applied in the work of Shi et al.[33] Such models are not able to describe some specific phenomena that occur in tanks exposed to severe fire conditions, such as liquid-phase thermal expansion during heat exposure.[12,34–36]

A specific structured approach to the problem was proposed by Venart and coworkers, which showed integral solution for equations governing free convection, continuity, momentum, and energy in vessels exposed to fires. The modeling studies were addressed at evidencing tank diameter effect on stratification[37] and at determining the dynamic evolution of the stratified boundary layer.[35] The use of distributed parameters codes to study the effect of fire exposure in LPG tanks was recently shown by Bi et al.,[38] which used FLUENT to determine the effect of different fire exposure configurations on small scale LPG tanks. Nevertheless, the detailed assessment of inner fluid behavior in large scale vessels during fire exposure with advanced tools for evaluating temperature stratification and liquid-phase thermal expansion during heat exposure is still lacking.

In the present study, a computational fluid dynamic (CFD) model is developed aimed at simulating the behavior of large scale LPG tankers exposed to fires. In particular, the CFD model is developed for horizontal cylindrical vessels fully engulfed in hydrocarbon pool fires. For this purpose, a two-dimensional (2-D) simulation is set up on ANSYS FLUENT code. The code is aimed at solving the conservation equations in a domain constituted by two continuous phases, for example, vapor and liquid. A specific user defined function (UDF) is implemented in the code in order to simulate in detail the condensation/evaporation phenomenon by evaluating mass and energy transfer between vapor and liquid. The CFD simulation is aimed at determining internal fluid temperatures and pressure, also evidencing in detail liquid stratification and thermal expansion phenomena.

The model predictions were compared and validated using available real scale experimental data.[39] The model was applied to case-studies derived from past accident data, in order to show the role of temperature distribution and liquid stratification in determining the pressure build-up and the time to failure of vessels exposed to fire.

Model

Theoretical background

Figure 1a summarizes the interacting processes which affect pressurized vessels storing liquefied gases during a fire attack. Although a section of a horizontal cylindrical vessel is shown in the figure, the fundamental phenomena involved are present in any type of vessel and geometry of industrial relevance.

A pressurized vessel exposed to fire receives heat due to radiation and convection. The heat load received is transferred by conduction through the vessel wall into the lading, causing the rise of vapor and liquid temperature and pressure. Natural convection governs the heat transfer from the vessel wall to the bulk of liquid and vapor phases. Initially, liquid–vapor equilibrium and a uniform temperature may be assumed. The heat transfer from the steel wall to the lading fluid causes the increase of the temperature of the fluid in contact with the portion of the vessels exposed to the fire. Significant heat dissipation occurs in the liquid with respect to the vapor due to the higher thermal conductivity. This, in turn, causes an upward flow of the hot liquid in the boundary layer in contact with the hot wall, and a downward flow in the central region of the liquid. The main effect of this gravity-driven recirculating flow is the formation of a vertical temperature gradient inside the tank: the liquid becomes thermally stratified. This phenomenon was extensively investigated in the past, through experiments[12,36] and theoretical studies.[29–33,37,38] Figure 1b schematizes the liquid phase stratification during the heat-up process.

As the liquid near the top of the tank will be at a higher temperature than the liquid downward, the vapor/liquid interface is formed by the warmest liquid layer of the stratified liquid zone. At the vapor/liquid interface, equilibrium conditions are satisfied, so the vapor at the interface is saturated

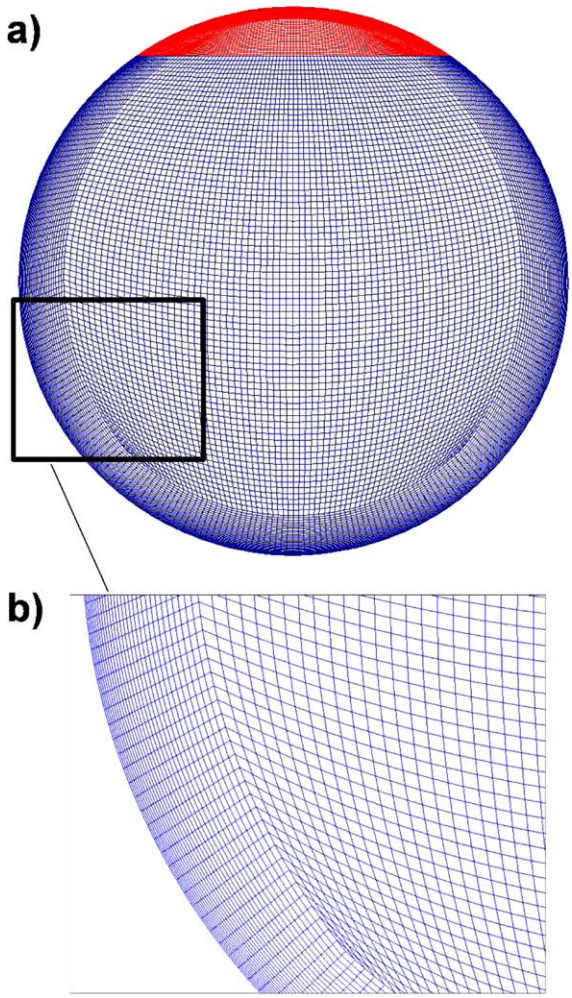

Figure 2. Calculation mesh adopted in the present study: (a) overview; (b) detail of a portion of the domain close to the vessel wall.

[Color figure can be viewed in the online issue, which is available at wileyonlinelibrary.com.]

at the temperature reached by the warmest liquid layer: the pressure in the tank, which is a critical parameter for the vessel resistance prediction, is therefore controlled by the warmest liquid.[12,29,36] To quantify the influence of thermal stratification on the vessel internal pressure, the dimensionless parameter Π is adopted[36]

$$\Pi = P/P^{\circ}(T_{\mathrm{L,av}}) \tag{1}$$

where P is the vessel internal pressure at a given fire exposure time and P° is the saturation pressure calculated at the average liquid temperature ($T_{\mathrm{L,av}}$).

Quite clearly, the higher Π, the higher the stratification effect on the internal tank pressure. Thus, in a thermally stratified liquid phase any critical pressure value, as the pressure relief valve (PRV) opening pressure is reached after a shorter time lapse than in a homogeneous liquid phase. Once generated, the thermal stratification continues affecting the stored liquid until other processes may take place, such as the PRV opening, that induces the mixing of the liquid phase dissipating the temperature gradients. Hence, stratification is a stable phenomenon that becomes more and more evident with time since the start of the fire exposure of the vessel.

Model development and implementation in a CFD code

To simulate the behavior of the internal fluid in vessels engulfed by fires, accounting for the phenomena previously outlined, a 2-D computational fluid dynamic (CFD) model was developed, aimed at solving the conservation equations in a domain representative of a horizontal cylindrical vessel section (see Figure 1). The domain is constituted by two continuous phases, for example, vapor and liquid. Several LPG commercial mixtures having different composition but similar overall properties are of industrial interest. In the present study, for the seek of simplicity, the properties of pure propane were assumed for calculations.

The following governing equations were implemented to evaluate the transient response of the pressurized vessel fully engulfed in fire

$$\frac{\partial \rho}{\partial t} + \nabla \cdot (\rho \mathbf{u}) = 0, \ \text{continuity equation} \tag{2}$$

$$\frac{\partial}{\partial t}(\rho e) + \nabla \cdot [\mathbf{u}(\rho e + P)] = E_e, \ \text{energy equation} \tag{3}$$

$$\frac{\partial}{\partial t}(\rho \mathbf{u}) + \nabla \cdot (\rho \mathbf{u}\mathbf{u}) = F_m, \ \text{momentum equation} \tag{4}$$

where ρ is the density, $\mathbf{u}$ is the velocity, P is the pressure, (ρe) is the total energy per unit volume, E_e contains the conduction term contribution to energy balance and the external energy source term, and F_m contains those parts of the stress term not explicitly shown due to external volumetric forces and gravity. Considering the temperatures that can be reached by the storage vessel wall while engulfed in fire, radiation between the steel wall was considered, assuming the stored fluid as a nonabsorbing media

$$\frac{\partial I_v}{\partial s} = 0, \ \text{radiative heat transfer equation} \tag{5}$$

where I_v is the incident radiation intensity on a single ray, s.

The governing equations were implemented in ANSYS FLUENT[40] V14.5 (FLUENT in the following) and solved for each control volume resulting from the spatial discretization of the physical domain. The ANSYS ICEM CFD software allows the construction of a structured mesh, and the use of its blocking tool enables refining the number of elements in the boundary layer near the vessel wall. The cells are topologically rectangular, thus cell volume is quadrilateral in 2-D domain. Figure 2 shows the overview (panel a) and a detail (panel b) of the mesh built for the present study, featuring 16,656 cells. A finer mesh (32,332 cells) is also built to verify that grid-independent predictions are obtained applying the mesh reported in Figure 2.

Governing Equations. Table 1 summarizes the main governing equations in transient turbulent regime solved for each control volume.

An Euler–Euler approach[42] was applied. The Eulerian method considers each different phase as an interpenetrating continuum: the volume of a phase cannot be occupied by the other phases. The CFD model accounts for transients tracking of temperature and pressure of vapor/liquid interface, then focuses on the transient thermal effects on the bulk stored fluid, evaluating temperature, and velocity associated to buoyancy driven flow.

Table 1. Governing Equations in Transient Turbulent Regime Implemented in the CFD Model

ID	Equation	Parameters Definition
A	$\frac{1}{\rho_L}\left[\frac{\partial}{\partial t}(\alpha_L\rho_L)+\nabla\cdot(\alpha_L\rho_L\mathbf{u}_L)=M_{CL}+M_{EL}\right]$	ρ_L: liquid density; t: time; α_L: liquid volume fraction; $\mathbf{u}_L$: liquid velocity; M_{CL}: condensation liquid-phase source term (see Eq. 12a); M_{EL}: evaporation liquid-phase source term (see Eq. 13a).
B	$\frac{\partial}{\partial t}(\rho e)+\nabla\cdot[\mathbf{u}(\rho e+P)]=\nabla\cdot(k_{eff}\nabla T)+S_E+S_C$	ρ: two-phase volume fraction averaged density (see Eq. F); e: two-phase averaged specific energy; $\mathbf{u}$: average velocity (see Eq. F); P: pressure; k_{eff}: effective thermal conductivity (see Eq. H); S_E: evaporation two-phase averaged source term (see Eq. 14a); S_C: condensation two-phase averaged source term (see Eq. 14b).
C	$\frac{\partial}{\partial t}\overline{[\rho(\bar{\mathbf{u}}+\tilde{\mathbf{u}})]}+\nabla\cdot\overline{[\rho(\bar{\mathbf{u}}+\tilde{\mathbf{u}})(\bar{\mathbf{u}}+\tilde{\mathbf{u}})]}=$ $-\nabla(P)+(\rho-\rho_o)\mathbf{g}+\nabla\cdot\left\{\mu\overline{\left[\nabla(\bar{\mathbf{u}}+\tilde{\mathbf{u}})+\nabla(\bar{\mathbf{u}}+\tilde{\mathbf{u}})^{\mathbf{T}}\right]}\right.$ $\left.-\frac{2}{3}\nabla\cdot\overline{\left[(\bar{\mathbf{u}}+\tilde{\mathbf{u}})\bar{\bar{\mathbf{I}}}\right]}\right\}+\mathbf{F}$	$\bar{\mathbf{u}}$: time averaged two-phase velocity; $\tilde{\mathbf{u}}$: time fluctuating two-phase velocity; μ: two-phase averaged viscosity (see Eq. F); ρ_o: reference density; $\mathbf{g}$: gravity acceleration; $\bar{\bar{\mathbf{I}}}$: identity tensor; $\mathbf{F}$: external volumetric forces term.
D	$\frac{\partial}{\partial t}(\rho K)+\nabla\cdot(\rho K\bar{\mathbf{u}})=\nabla\cdot[(\mu+\frac{\mu_T}{\sigma_K})\nabla K]+\chi_1-\rho\varepsilon+S_K$	K: turbulence kinetic energy; μ_T: two-phase averaged turbulence viscosity (see Eq. F); $\sigma_K=1.00$ turbulence standard K-ε model constant[41]; χ_1: production and destructions terms for turbulence kinetic energy[41]; ε: turbulence dissipation rate; $S_K=0$, turbulence kinetic energy source term.
E	$\frac{\partial}{\partial t}(\rho\varepsilon)+\nabla\cdot(\rho\varepsilon\bar{\mathbf{u}})=\nabla\cdot[(\mu+\frac{\mu_T}{\sigma_\varepsilon})\nabla\varepsilon]+C_{1\varepsilon}\frac{\varepsilon}{K}\chi_2-C_{2\varepsilon}\rho\frac{\varepsilon^2}{K}+S_\varepsilon$	$\sigma_\varepsilon=1.30$, $C_{1\varepsilon}=1.44$; $C_{2\varepsilon}=1.92$; are the turbulence standard K-ε model constants[41]; χ_2: production and destruction rate for turbulence dissipation rate[41]; $S_\varepsilon=0$, turbulence dissipation rate source term.
F	$\zeta=\alpha_L\zeta_L+(1-\alpha_L)\zeta_V$	Two-phase volume fraction averaged property ζ function of liquid and vapor properties (ζ_L and ζ_V, respectively, where ζ can be substituted by density ρ, dynamic viscosity μ, turbulent viscosity μ_T, thermal conductivity k, velocity $\mathbf{u}$).
G	$\xi=\frac{\alpha_L\rho_L\xi_L+(1-\alpha_L)\rho_V\xi_V}{\alpha_L\rho_L+(1-\alpha_L)\rho_V}$	Two-phase mass averaged property ξ function of liquid and vapor properties (ξ_L and ξ_V, respectively, where ξ can be substituted by: temperature T, energy per unit mass e, heat capacity c_p)
H	$k_{eff}=k+\frac{c_p\mu_T}{Pr_T}$	k = two-phase volume fraction averaged thermal conductivity (see Eq. F); c_p: two-phase volume fraction averaged heat capacity (see Eq. G); $Pr_T=0.85$, turbulent Prantl number assumed as constant.[41]
I	$\mu_T=\frac{\rho C_\mu K^2}{\varepsilon}$	$C_\mu=0.09$ turbulence standard Kε model constant.[41]

A critical issue in the implementation of the main governing equation is associated to Eq. 2 (continuity equation). In fact, in the present case, the vapor/liquid interface rises due to liquid vaporization, but the Eulerian calculation assumes a constant value of interface level. Therefore, the Eulerian volume of fluid method[43] (VOF) was introduced, based on the assumption that in each control volume the phases considered are characterized by a volume fraction that is assumed to be a continuous function of space and time. Therefore, given the liquid and vapor volume fractions, respectively, α_L and α_V, the following condition must be verified among the entire calculation domain

$$\sum_{\text{domain}}(\alpha_L+\alpha_V)=1 \tag{6}$$

In the present study, in which a two-phase system is considered, the VOF assumption allows solving the continuity equation only for one phase, for example, only in terms of α_L as reported in Table 1 (see Eq. A). After the evaluation of α_L, the vapor fraction α_V in each control volume is obtained by applying Eq. 6.

Energy equation is solved throughout the computational domain. At the interface, liquid and vapor are in equilibrium, hence at the same temperature (see Table 1). Actually, the VOF model treats the temperature and the total energy as mass averaged variables, while all the other fluid properties at the interface are computed as volume-fraction averaged variables.

In analogy with the case of energy equation, a single set of momentum equations is solved throughout the computational domain. Previous studies demonstrated that natural convection boundary layer in enclosures turns from laminar to turbulent regime faster than natural convection boundary layer for vertical semi-infinite walls.[44] As a matter of fact, in several works dealing with modeling studies of vessels exposed to external heat sources, turbulent natural convention flow was predicted.[15] Therefore, a turbulence model was used since the start of the CFD simulation. In particular, the equation of motion was solved with the standard turbulence kinetic and turbulence dissipation rate model (Standard K-ε).[43] This well-known approach was adopted by several researchers and details are extensively discussed elsewhere.[45]

The VOF model obtains the motion of interface indirectly by determining the motion of all the two phases. In a 2-D domain, the interface is considered to be a piecewise continuous line.[46] To represent the interface, the mathematical piecewise polynomial approach provided by the geometric reconstruction interpolation scheme[46] is used.

Finally, radiative heat transfer among the liquid phase is neglected, following the approach of several previous studies[29–33,37,38] which identify natural convection and nucleate

Table 2. Correlations Adopted in the Present Study for the Evaluation of Propane Physical Properties

Item	Units	Correlation	Notes
Liquid density (ρ_L)	kg m^{-3}	$\rho_L = -24.063 + 4.9636T - 0.0109T^2$; T in K	(A)
Vapor density (ρ_V)	kg m^{-3}	See Table 3	
Liquid heat capacity (c_{pL})	J kg^{-1} K^{-1}	$c_{pL} = 36309 - 230.2T + 0.3941T^2$; T in K	(A)
Vapor heat capacity (c_{pV})	J kg^{-1} K^{-1}	$c_{pV} = 168.03 + 5.6056T - 0.0014T^2$; T in K	(B)
Liquid thermal conductivity (k_L)	W m^{-1} K^{-1}	$k_L = 0.26755 - 6.60\times10^{-4}T + 2.77\times10^{-7}T^2$; T in K	(A)
Vapor thermal conductivity (k_V)	W m^{-1} K^{-1}	$k_V = -0.0088 + 6.00\times10^{-5}T + 1.00\times10^{-7}T^2$; T in K	(A)
Liquid dynamic viscosity (μ_L)	Pa s	$\mu_L = 709137T^{-3.986}$; T in K	(A)
Vapor dynamic viscosity (μ_V)	Pa s	$\mu_V = 4.9054\times10^{-8}T^{0.90125}$; T in K	(A)
Saturation temperature (T°)	K	$T^\circ = 253.76 + 5.0\times10^{-5}P - 6.0\times10^{-12}P^2$; P in Pa	(A)
Saturation heat of vaporization (λ°)	J kg^{-1}	$\lambda^\circ = 403262 + 0.0682P$; P in Pa	(A)

(A) Interpolation of data reported by Liley et al.[54]
(B) Interpolation of data reported by Townsend et al.[39]

boiling as the more important mechanisms of heat transfer in the liquid space. The radiation in the top vapor space is instead considered introducing the S2S (surface to surface radiation) model assuming the vapor as a nonparticipating medium. More details on the S2S model are reported elsewhere.[47,48]

Condensation/Evaporation Subroutine. To simulate in detail the condensation/evaporation phenomenon, which is critical for the assessment of the present two-phase system, a specific UDF was developed in C++ code, interpreted by the CFD software and implemented for the simulations. The UDF calculates the mass transfer and the related energy transfer due to evaporation–condensation process using the Hertz–Knudsen equation[49]

$$J = \beta_C \sqrt{\frac{M_w}{2\pi R}} \left(\frac{P}{\sqrt{T_V}} - \frac{P^\circ}{\sqrt{T_L}} \right) \tag{7}$$

where T_V and T_L are the vapor and liquid temperatures, β_C is the accommodation condensation coefficient, representing the ratio between the experimentally observed condensation velocity and the maximal theoretical condensation velocity. The same definition is extended to the evaporation accommodation coefficient, β_E. Under saturation conditions, saturated pressure and temperature are linked by Clausius–Clapeyron equation[50]

$$(P - P^\circ) = -\frac{\lambda^\circ}{T\left(\frac{1}{\rho_V} - \frac{1}{\rho_L}\right)} (T - T^\circ) \tag{8}$$

Substitution of Eq. 8 in Eq. 7 results in

$$J = \beta_C \sqrt{\frac{M_w}{2\pi R T^\circ}} \frac{\lambda^\circ}{\left(\frac{1}{\rho_V} - \frac{1}{\rho_L}\right)} \frac{(T^\circ - T)}{T^\circ} \tag{9}$$

Once J is obtained, the mass sources connected to the condensation or evaporation process implemented in the continuity equation (see Eq. A, Table 1) are evaluated estimating the volumetric interfacial surface area (a_L and a_V for liquid and vapor phases), which can be expressed as a function of the mean Sauter diameter[51] (D_{MS}) and the volume fraction (α) of the phase under consideration, assuming spherical bubbles

$$a_L = \frac{6\alpha_L}{D_{MS}}; a_V = \frac{6\alpha_V}{D_{MS}} \tag{10}$$

Hence, the mass source terms due to condensation and evaporation, respectively, X_{CL} and X_{EV} are expressed combining Eqs. 9 and 10

$$X_{CL} = \left[\beta_c \frac{6}{D_{MS}} \sqrt{\frac{M_w}{2\pi R T^\circ}} \frac{\rho_L \lambda^\circ}{(\rho_L - \rho_V)} \right] \rho_V \alpha_V \frac{(T^\circ - T)}{T^\circ} = \beta'_C \rho_V \alpha_V \frac{(T^\circ - T)}{T^\circ} \tag{11a}$$

$$X_{EV} = \left[\beta_e \frac{6}{D_{MS}} \sqrt{\frac{M_w}{2\pi R T^\circ}} \frac{\rho_V \lambda^\circ}{(\rho_L - \rho_V)} \right] \rho_L \alpha_L \frac{(T^\circ - T)}{T^\circ} = \beta'_E \rho_L \alpha_L \frac{(T^\circ - T)}{T^\circ} \tag{11b}$$

The terms β'_C and β'_E are the mass-transfer time relaxation parameters and represent the rate of condensation and evaporation. According to the work of Wu et al.,[52] the

Table 3. Equation of State for Propane Implemented in the CFD Model[50]

Item	Units	Equation/Value
Vapor density (ρ_V)	g cm^{-3}	$\rho_V = M_w\ 10^3\ v_m^{-1}$
Peng–Robinson equation of state (v_m evaluation)	cm^3 mol^{-1}	$P = \frac{RT}{v_m - b} - \frac{a\psi}{v_m^2 + 2bv_m - b^2}$
Universal gas constant (R)	cm^3 bar mol^{-1} K^{-1}	8.314413
First Peng–Robinson equation coefficient (a_{PR})	–	$a_{PR} = \frac{0.45724R^2T_c^2}{P_c}$
Second Peng–Robinson equation coefficient (b_{PR})	–	$b_{PR} = \frac{0.07780RT_c}{P_c}$
Peng–Robinson parameter (ψ)	–	$\psi = \left\{ 1 + (0.37464 + 1.54226\omega - 0.26992\omega^2)\left[1 - \left(\frac{T}{T_c}\right)^2\right] \right\}$
Molar mass (M_w)[a]	g mol^{-1}	44.10
Critical temperature (T_c)[a]	K	369.9
Critical pressure (P_c)[a]	bar	42.051
Acentric factor (ω)[a]	–	0.152

[a]Propane physical properties implemented in Peng–Robison equation are derived from Liley et al.[54]

Table 4. Parameters Adopted in the CFD Model Set Up for the Validation

Item	Selected Parameter/Value
Primary phase	Vapor phase
Patched variable	Liquid phase volume fraction
Under-relaxation factors	0.30; 1.00
Convergence criteria	10^{-6}
Time step (s)	0.03

value of these parameters may be set equal to 0.1. Considering that the condensation process decreases the amount of the vapor phase while the evaporation process increases it, and considering positive an incoming mass-transfer rate, the mass source terms expressions in the UDF (see Table 1) are:

1. for condensation, occurring at $T_v < T^\circ$

$$M_{CL} = 0.1\rho_V\alpha_V\left|\frac{(T_v - T^\circ)}{T^\circ}\right|, \quad \text{(12a)}$$

source term increasing liquid phase mass

$$M_{CV} = -M_{CL} = -0.1\rho_V\alpha_V\left|\frac{(T_v - T^\circ)}{T^\circ}\right|, \quad \text{(12b)}$$

source term decreasing vapor phase mass

2. for evaporation, occurring at $T_L > T^\circ$

$$M_{EL} = -0.1\rho_L\alpha_L\left|\frac{(T_L - T^\circ)}{T^\circ}\right|, \quad \text{(13a)}$$

source term decreasing liquid phase mass

$$M_{EV} = -M_{EL} = 0.1\rho_L\alpha_L\left|\frac{(T_L - T^\circ)}{T^\circ}\right|, \quad \text{(13b)}$$

source term increasing vapor phase mass

Therefore, implementing Eqs. 12 and 13 in the continuity equation allows quantifying the correct interphase mass source term for both the liquid and vapor phase. For what concern the energy balance and the estimation of the heat transfer during the evaporation or condensation process, only one expression is required (see Eq. B Table 1), in which the energy source terms related to evaporation (S_E) and condensation (S_C) are expressed as follows

$$S_E = \lambda^\circ M_{EL}, \text{ energy source term associated to the evaporation in the control volume} \quad \text{(14a)}$$

$$S_C = \lambda^\circ M_{CV}, \text{ energy source term associated to the condensation in the control volume} \quad \text{(14b)}$$

In the present UDF, both the saturation temperature and the latent heat of vaporization are a function of the pressure of the domain, which changes with time. It is also worth to mention that the UDF is specifically aimed at the calculation of mass and energy transfer between vapor and liquid due to evaporation–condensation process. The UDF does not assume any momentum exchange between the two phases: source terms contribution to momentum, turbulence kinetic energy, and turbulence dissipation rate are set equal to zero (see Table 1).

Equation of State and Physical Properties Implemented in the Simulations. As stated above, the LPG stored in the vessels exposed to the fire is assumed as pure propane, neglecting the presence of heavier components, such as butane, according to the typical US and Canada composition.[1,53] The physical properties of the liquid and the vapor propane were implemented as a function of temperature (see Table 2).

To improve FLUENT computational performance, simplified correlations were built as polynomial functions, interpolating available thermodynamic data (see Table 2) for all the liquid and vapor relevant properties except for the dynamic viscosity. For this parameter, the dependence on temperature was modeled using a power law. The vapor density was solved using the Peng–Robinson Equation of State,[50] implemented in the FLUENT software[40] (see Table 3).

Turbulence models. In the present numerical simulations, a two-equation model is chosen for Reynolds Stresses: the Standard K-ε turbulence model. This well-known approach was adopted by several researchers and details are extensively discussed elsewhere.[41,45,55]

The numerical model takes also into account the presence of the steel solid wall of the vessels and its influence on the fluid flow. Close to the wall, the flow is induced by viscous effects and does not depend on free stream parameters: it only depends on the orthogonal distance from the wall. The FLUENT tool used to model the near wall region is the wall function approach. The use of wall functions obviates the

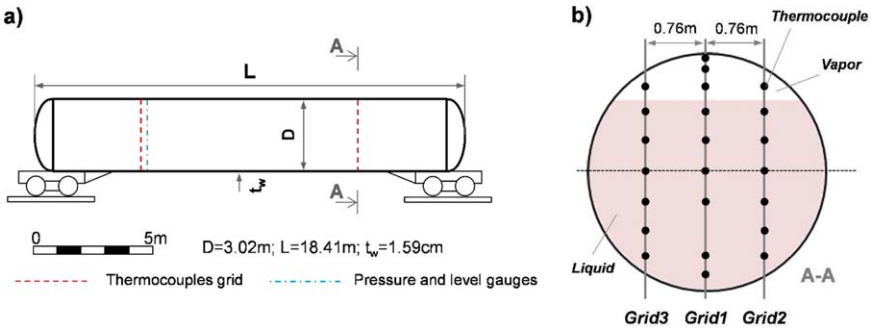

Figure 3. (a) Overview of the tanker used in the validation experiment; (b) location of thermocouples. Adapted from Ref. 39.

[Color figure can be viewed in the online issue, which is available at wileyonlinelibrary.com.]

Table 5. Boundary and Initial Conditions Implemented in the FLUENT Simulations

Item	Selected Parameter/value	
	Validation Study and Case Study A	Case Study B
Initial Temperature	294.15 K	294.15 K
Initial Pressure	0.963 MPa	0.963 MPa
Fire condition for the wall in contact with the liquid[a]	45,196 W/m^2	100,000 W/m^2
Fire condition for the wall in contact with the vapor[a]	1144.15 K	1144.15 K

[a]Constant heat flux is imposed on the vessel wall in contact with the liquid; radiative heat source at constant temperature is applied on the vessel wall in contact with the vapor.

need to modify the turbulence models to account for the presence of the wall. More details on the use of wall function approach and accurateness of the method are discussed elsewhere.[41,55]

Set Up of CFD Simulations in FLUENT. As previously outlined, the multiphase VOF method is used in the FLUENT simulations. Therefore, the available numerical techniques and solution tools were selected to promote the stability of the overall solution process. The main parameters for the CFD simulations set-up are summarized in Table 4.

SIMPLE transient pressure-velocity coupling algorithm was applied, and body force weighted pressure spatial discretization scheme was used, while all the other fluid physical properties were spatially discretized using a first-order discretization scheme. Time discretization was achieved with first-order Euler implicit method. All the numerical simulations were performed on a DELL-OPTIPLEX 9010 PC, with INTEL® CORE™ i7-3370, CPU @3.40 GHz, 16 GB RAM, and 64 bit operating system type. Parallel calculation was performed with four cores, requiring 200 MB memory in order to obtain a computational time of about 20 min to simulate 1 s real time.

Model Validation and Case-Studies

Experimental data available for model validation

The experimental data obtained in the large scale bonfire test performed by Townsend et al.[39] are taken as a reference data source for model validation. In the test considered, a propane tank car was exposed to a complete engulfment in a hydrocarbon pool fire. The tank car complied with the DOT 112A340W specification,[56] according to the US regulation for the transportation of liquefied pressurized gases (such as LPG, anhydrous ammonia, and vinyl chloride) and had a nominal capacity of 125 m^3. Figure 3a shows a sketch of the tank car tested. A PRV, with an opening pressure set to 1.816 MPa, was installed to protect the tanker, which was not provided with thermal insulation. The tested tank was almost full of liquid at the beginning of the test (96% by volume). At the beginning of the test, all the vessel and internal fluids were at ambient temperature.

Several parameters were measured during the tests. Figure 3b shows the grid of Chromel Alumel Thermocouples (precision ±2.2°C) positioned inside the tank to monitor the internal fluid and the lading temperature. In particular, the thermocouples where positioned on three vertical lines (namely, Grid1, Grid2, and Grid3, see Figure 3b). Six pressure gauges were installed inside the tank to monitor the vessel pressure data. Gauges were also used to monitor the liquid level as a function of time. No specification is reported by Townsend et al.[39] about the precision of these instruments.

A radiometer (range 0–1255 kW/m^2, accuracy 1%) was used to monitor the external radiative heat flux. Ten external Chromel Alumel thermocouples (precision ±2.2°C) were installed to measure the fire temperature.

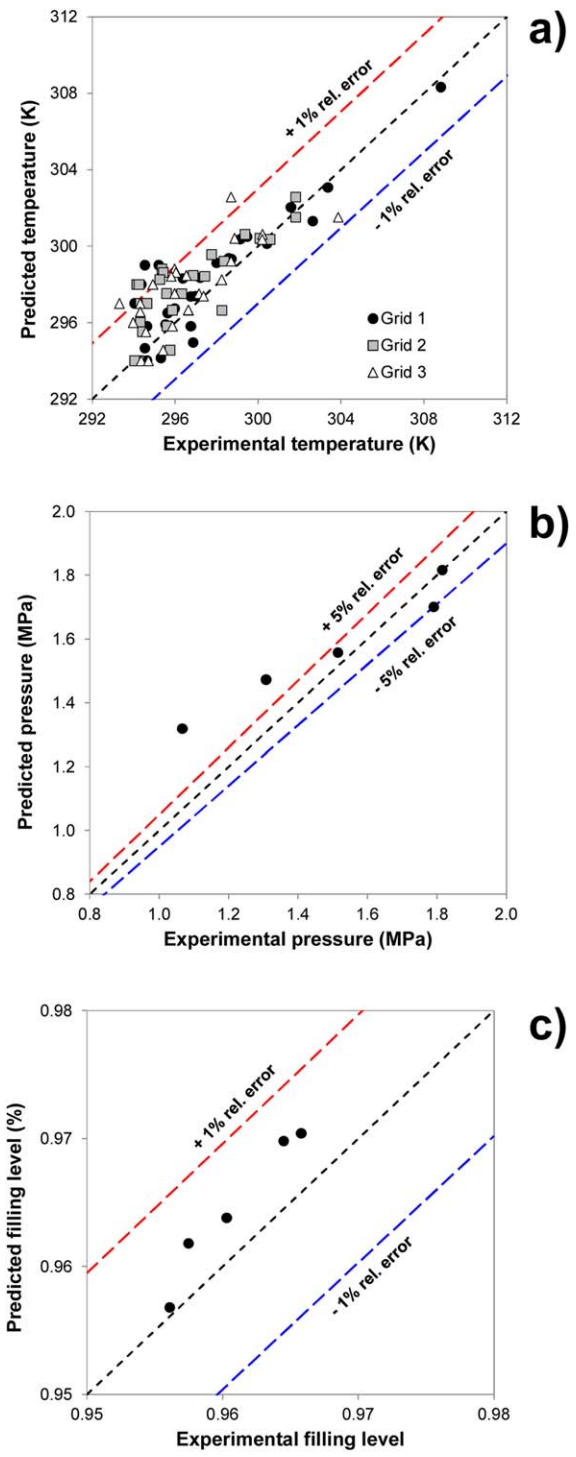

Figure 4. Results of model validation. Parity plots for: (a) experimental and predicted temperatures (K); (b) pressure in MPa; (c) liquid level, expressed in terms volumetric fraction.

[Color figure can be viewed in the online issue, which is available at wileyonlinelibrary.com.]

Table 6. Comparison between Experimental and Predicted Temperatures for the Validation Case: Average Absolute (η_{abs})[a] and Relative Error (η_{rel})[a] for Different Simulated Fire Exposure Times for each Thermocouple Grid

	Grid 1		Grid 2		Grid 3	
Time (s)	η_{abs} (K)	η_{rel} (%)	η_{abs} (K)	η_{rel} (%)	η_{abs} (K)	η_{rel} (%)
52	1.9	0.65	2.0	0.68	1.7	0.59
70	0.3	0.11	1.6	0.53	1.7	0.57
95	0.3	0.11	1.0	0.34	0.7	0.23
113	0.1	0.05	0.4	0.14	0.3	0.11

[a]$\eta_{abs} = T_{mod} - T_{exp}$, $\eta_{rel} = 100 \times (T_{mod} - T_{exp})/T_{exp}$ where T_{mod} and T_{exp} are, respectively, the model and experimental temperatures.

On the basis of the experimental parameters measured during the tests, it was possible to assume the initial and boundary conditions summarized in Table 5 for CFD simulation. The boundary conditions are aimed at simulating a uniform full engulfment on the external tank surface. A constant heat flux is imposed on the wall in contact with the liquid, based on an average value obtained by the analysis of radiative heat flux measurement during the first 132 s of the fire test. A radiative heat source at constant temperature, obtained as the average value of fire temperature measured during the test, is applied on the vessel wall in contact with the vapor.

Case-studies selected for model application

To assess its potentialities, the model was applied to some case-studies of industrial interest. In all the case-studies analyzed, the same tank geometry and the same geometrical features of the tank used for the large scale bonfire test performed by Townsend et al.[39] and summarized in Figure 3 were used. A sensitivity analysis on the boundary and operative conditions was carried out by analyzing two reference case-studies:

- Case-study "**a**": same input heat flows of the validation case (VC), but lower liquid filling level (set to 50%) in order to show the effect of the liquid hold up reduction on the thermal stratification;
- Case-study "**b**": higher thermal heat flows, to reproduce a fully developed fire (100 kW/m^2) and a more severe fire attack with the same liquid filling level of the VC.

Table 5 summarizes the boundary conditions imposed for the two case studies. In both cases, uniform fire engulfment was considered.

Results and Discussion

Model results for the validation case (VC)

The results obtained for the VC are shown in Figure 4.

The figure reports three parity plots in which the model predictions are compared with the experimental results obtained by Townsend et al.[39] Figure 4a shows the temperature data. The comparison was possible only before the opening of the PRV, thus only few measurements are available for the three thermocouples grids shown in Figure 3. The CFD results are in good agreement with the experimental data, thus allowing an accurate prediction of the liquid stratification process associated to the vessel heat up and schematized in Figure 1. Figure 4a also reports two buffer lines delimitating the zone in which the relative error between predicted and measured values ranges between −1 and +1%. Only few CFD results fall outside this area, mainly at lower temperatures. To better characterize the quality of model predictions, an error analysis is reported in Table 6. For each data acquisition time, Table 6 shows the average absolute and relative error of the CFD model predictions for each temperature grid. As shown in the table, the model allows for an accurate prediction of the inner fluid temperature.

The same type of comparison is shown in Figure 4b for pressure predictions, while Table 7 shows the analysis of model errors. In this case, some discrepancies are found between model values and experimental data, with an average absolute error of 0.07 MPa and an average relative error equal to 6.75%. The model overestimation of the internal pressure may be related to the assumption of equilibrium conditions at the vapor/liquid interface. In the CFD model, the vapor at the interface is supposed to always have a temperature equal to that of the hotter liquid layer, neglecting the effects of thermal inertia, which causes a delay in the vapor heat up and, thus, in the pressure increase, not accounted in CFD model predictions. As a matter of fact, as shown in Figure 4b, when heat transfer into the vapor is more efficient, thus when vapor heats up after a prolonged fire exposure, more accurate predictions are obtained for pressure, thus allowing a precise estimation of the PRV opening time, that is a key issue for the assessment of pressurized vessels resistance to fire exposure.[29–33,37,38] Actually, in the CFD simulation, the PRV opens after 132.6 s from fire start, whereas in the experimental test, the PRV opened after 132.0 s.

Table 7. Comparison between Experimental and Predicted Pressure and Filling Level for the Validation Case: Absolute (η_{abs})[a] and Relative Error (η_{rel})[a] for Different Simulated Fire Exposure Times

	Pressure Prediction			Filling Level Prediction	
Time (s)	η_{abs} (MPa)	η_{rel} (%)	Time (s)	η_{abs} (-)	η_{rel} (%)
30	0.251	23.5	29.36	0.0007	0.07
60	0.164	12.5	61.96	0.0043	0.45
90	0.042	2.8	89.91	0.0035	0.36
120	−0.091	−5.1	117.84	0.0053	0.55
132	0	0.0	122.49	0.0046	0.48

[a]$\eta_{abs} = \Xi_{mod} - \Xi_{exp}$; $\eta_{rel} = 100 \times (\Xi_{mod} - \Xi_{exp})/\Xi_{exp}$ where Ξ_{mod} and Ξ_{exp} are, respectively, the model and experimental parameters (pressure or filling level).

Table 8. Quantification of the Discrepancies between "Fine" (32,332 Cells) and "Coarse" Mesh (16,656 Cells, Adopted in the Present Study): Average Relative Error (η_{rel})[a] for Different Predicted Quantities

Predicted Quantity	Average Relative Error[a] (%)
Temperature grid 1	0.072
Temperature grid 2	0.105
Temperature grid 3	0.059
Pressure	0.774
Filling level	0.147

[a]$\eta_{rel} = 100 \times (\Xi_{cr} - \Xi_{fn})/\Xi_{fn}$ where Ξ_{cr} and Ξ_{fn} are, respectively, the quantities predicted with "fine" and "coarse" mesh.

Figure 4c shows the comparison between the predicted and measured volumetric filling level. Table 7 reports the relative error calculated for model predictions with respect to experimental data. As evident from the table, relative error is always lower than 1%, with an average absolute error of 0.004 in the value of the volumetric fraction. As evident from Figure 4c, the thermal expansion occurring in the liquid phase is slightly overestimated by the model, without affecting internal pressure predictions.

To verify the quality of the grid adopted in the present study, Table 8 reports the discrepancies of the results obtained with the mesh depicted in Figure 2 (16,656 cells) respect to the ones obtained with the finer mesh (32,332 cells). In particular, the relative average error in temperature, pressure, and filling level prediction is shown, demonstrating a limited variation of the results and thus the adequacy of the coarser mesh.

It may be concluded that overall a rather good agreement was found between the CFD model predictions and the results of the large-scale bonfire test considered.

Results of case-studies

The sensitivity of the CFD model to some critical parameters was tested by the application to case-studies. Figure 5 shows the results obtained in the analysis of case-study "**a**," where a lower filling level (50%) was considered.

Figure 5a shows the liquid temperature distribution at the beginning of the fire exposure. For the sake of clarity, the temperature of the vapor phase is not reported, in order to show the boundary of vapor/liquid interface evolution. As expected, the liquid stratification only occurs in layer that is about 20 cm thick, in the proximity of the vapor/liquid interface, with temperatures ranging between 305 and 326 K. This corresponds to a temperature gradient of about 105 K/m along the vessel vertical axis. The map also shows the thermal boundary layer that is formed near to the vessel wall exposed to fire, which results in the liquid recirculation to the hot upper layer. This is confirmed by the analysis of the axial velocity profile shown in Figure 5b, in accordance with the schematization reported in Figure 1b. In fact, while the liquid in contact with the wall reaches the upper hot layer, the cooler liquid moves downward, accumulating in the cooler bulk zone, in which the temperature ranges between 300 and 307 K. Thus, an extremely lower temperature gradient is present with respect to the upper part of the tank (about 5 K/m along the vessel vertical axis). However, at the bottom of the vessel, an unstable zone appears due to fire exposure. Hence, the liquid is forced to recirculate by natural convection. This phenomenon leads to a rapid liquid heat up. As shown in Figure 5c after 450 s of fire exposure, a homogenous temperature distribution is present all over the liquid phase (overall temperature gradient is as low as 10 K/m along the vessel vertical axis). Due to the lower temperature and density difference, liquid velocity drastically decreases

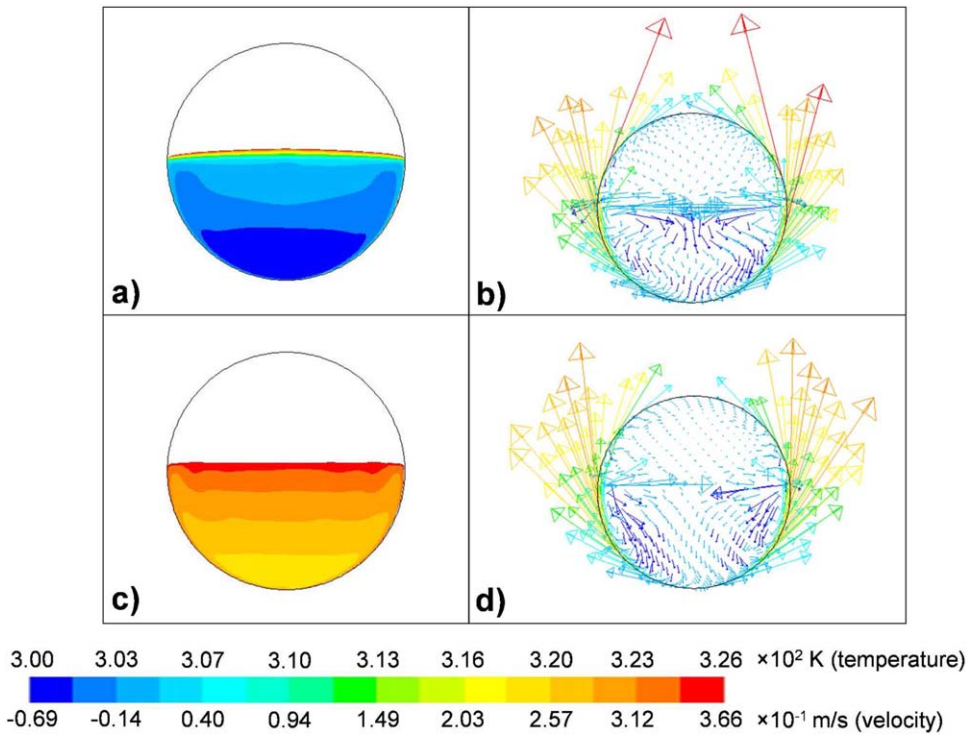

Figure 5. CFD results for case-study "a": temperature profile (K) at 150 s (a) and 450 s (c); axial velocity profile (in m/s) at 150 s (b) and 450 s (d).

[Color figure can be viewed in the online issue, which is available at wileyonlinelibrary.com.]

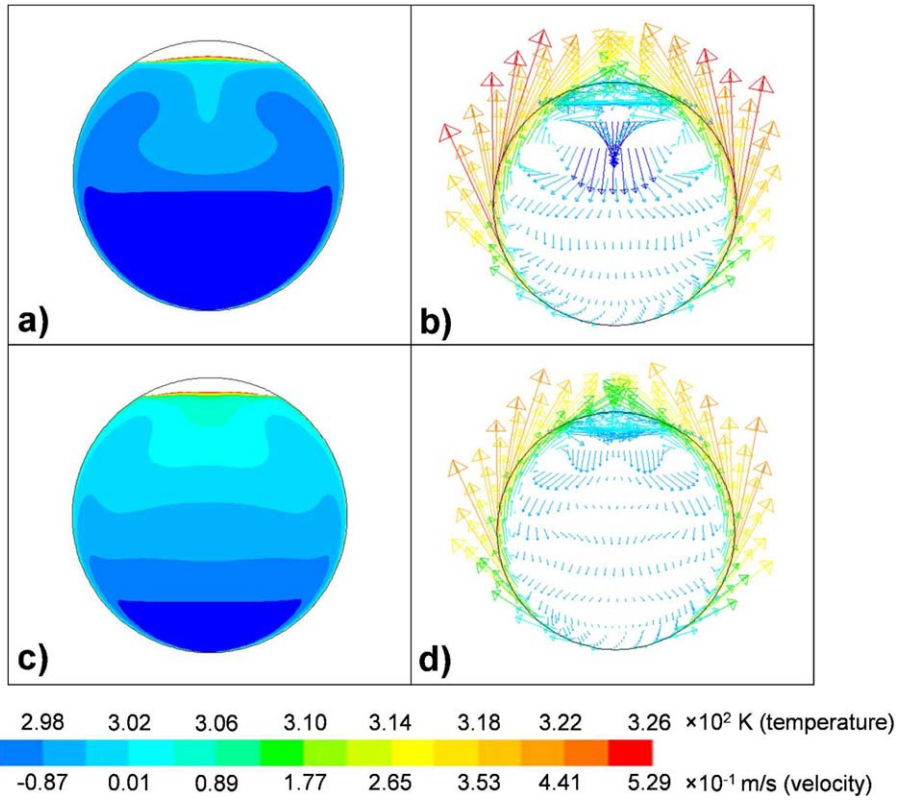

Figure 6. CFD results for case-study "b": temperature profile (K) at 30 s (a) and 60 s (c); axial velocity profile (in m/s) at 30 s (b) and 60 s (d).

[Color figure can be viewed in the online issue, which is available at wileyonlinelibrary.com.]

in the bulk (see Figure 5d), while the recirculation occurs only close to the vessel wall.

Figure 6 shows the results obtained for case study "**b**," where more severe fire conditions, resulting in a higher heat flow, are considered.

The liquid stratification appears in a smaller portion of the liquid with respect to case study "**a**." In fact, after 30 s of fire exposure (see Figure 6a), the hot layer close to the vapor/liquid interface is about 6 cm thick, with temperature ranging between 326 and 308 K, while more than half of the liquid in the vessel is almost at its initial temperature (between 294 and 296 K). The upper part of the vessel is characterized by the formation of the same type of recirculation phenomena obtained in case study "**a**," but with higher velocities (about two times those of the previous case, as shown in Figure 6b). After 60 s of fire exposure, a pronounced stratification is still present in the liquid. The thickness of the hot upper layer is increased (about 35 cm), and significant recirculation velocities are predicted (see Figure 6d). Case study "**b**" demonstrates that the pressure build-up in the vessel is strongly affected by the formation of a thermally stratified liquid layer. In this case, due the higher heat load, this phenomenon is more rapid, leading to a faster pressure increase and the consequent PRV opening after only 65 s since fire start: less than half of the time required in case-study "**a**," in which less severe fire conditions were considered.

Discussion

The results obtained show the importance of the dynamic liquid temperature profiles in a vessel exposed to fire and their influence on the internal pressure build-up. To highlight this issue, the stratification index, Π, defined in Eq. 1, was evaluated postprocessing the CFD results. Figure 7 shows the comparison among Π, internal pressure (P), and average liquid temperature ($T_{L,av}$) calculated, respectively, for the VC (Figure 7a), case study "**a**" (Figure 7b), and case study "**b**" (Figure 7c).

As shown in Figure 7, the dynamic pressure behavior is characterized by a nonregular growth, with significant changes in the slope of the pressure curves. This is due to the transient effect associated to the different thermal inertia of liquid and vapor phases. In fact, the liquid at the interface needs time to heat up and to reach saturation conditions, thus delaying the pressure growth inside the vessel.

Reducing the volumetric liquid filling level from 96 to 50%, a significant difference in the stratification behavior is predicted. If the first 65 s of simulation are considered, in which all the three cases can be compared, the average liquid temperature, $T_{L,av}$, is similar in all the three cases considered (i.e., about 297 K after 65 s) due to the limited heat-up. However, while for high filling levels, the Π index features a rapid growth in time with similar rates (i.e., 7.06×10^{-3} and 9.88×10^{-3} s^{-1}, respectively, for VC and case study "**b,**" as shown in Figures 7a, c), for the lower filling level considered in case-study "**a**" a smaller rate is obtained (1.58×10^{-3} s^{-1} as shown in Figure 7a, about five times slower with respect to the previous cases). Hence, in the latter case stratification is less pronounced and the liquid is more homogenous due to the lower "thermal inertia" of the system, characterized by a lower liquid hold up with respect to the previous cases.

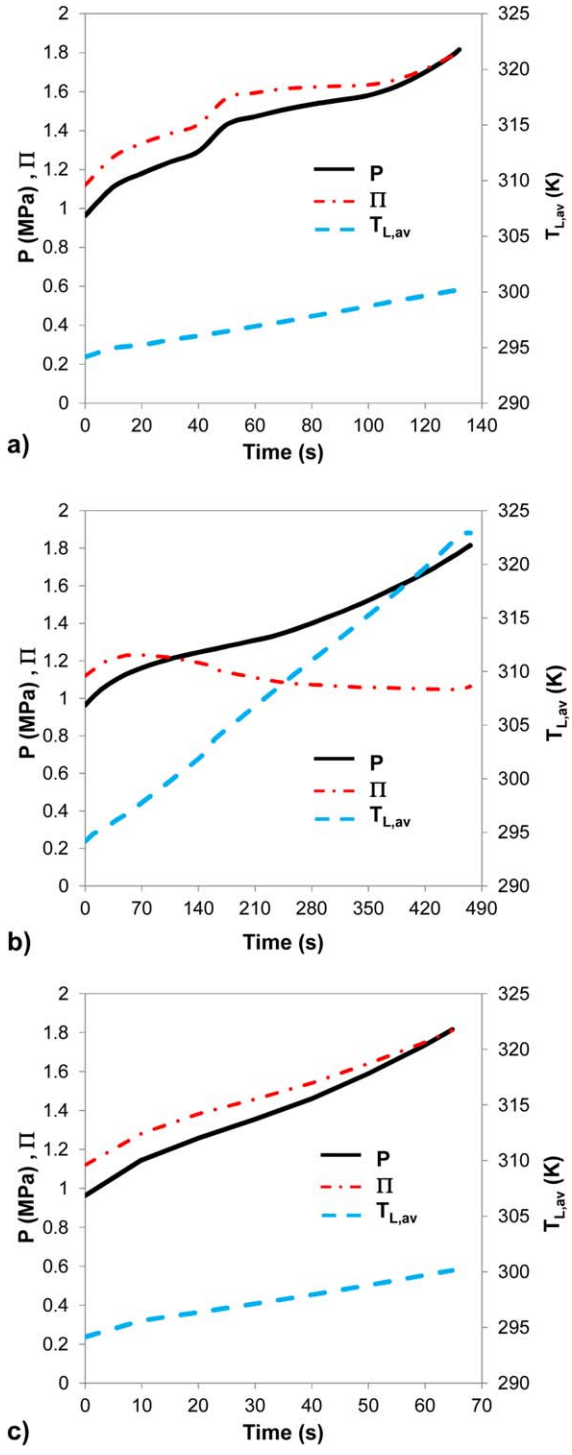

Figure 7. Average liquid temperature ($T_{L,av}$), pressure (P), and dynamic stratification index (Π) for: (a) validation case; (b) case-study "a"; (c) case-study "b."

[Color figure can be viewed in the online issue, which is available at wileyonlinelibrary.com.]

In case study "**a,**" a gradual and slower vessel pressurization is obtained. Thus, predicted PRV opening time (476 s) is much higher than in the other cases considered: 132 s in the VC, where the same heat load is considered, and 65 s in case study "**b**," where a higher heat load is assumed.

Therefore, for higher liquid filling levels, the stratification has a more relevant effect on internal pressure increase. The results show that for high liquid hold-up values, the internal pressure is related to the temperature of the upper warm liquid layer rather than to the average bulk temperature. In case study "**b**," this effect is more pronounced, as the fire heat load is doubled with respect to the VC. On the contrary, reducing the liquid hold up allows for a lower liquid stratification and thus the pressure growth is mostly influenced by the average liquid temperature. This is in accordance with experimental findings obtained in small scale bonfire tests.[57–59]

It should be remarked that in case study "**a**" the delayed pressurization allows a longer duration of the simulation with respect to the previous cases. In the final part of the simulation, Π decreases to a constant plateau (see Figure 7a), while the average liquid temperature increases to 323 K. This indicates that in the latter case, the stratification only occurs during the initial heat-up, while a more homogenous medium is obtained after a prolonged fire exposure.

The top space volume also influences the internal pressure growth, due to liquid thermal expansion, which, on turn, is associated to liquid temperature increase. To investigate this issue, Figure 8 reports the comparison between the predicted liquid level transient due to liquid thermal expansion until the PRV opening time calculated for the VC and for case-studies "**a**" and "**b**."

The transient effects that were found in the pressure build up in the vessel (see Figure 7) also affect the temperature rise in the liquid and, thus, the thermal expansion behavior, which features a nonregular growth. As clearly shown in the figure, liquid thermal expansion is more pronounced in case study "**a**." Nevertheless, this has a limited influence on the internal pressure, as the vapor space is half of the total vessel volume. On the contrary, even if the thermal expansion is lower for the VC and case study "**b**," a more relevant effect is found on vessel internal pressure, due to the higher influence of liquid thermal expansion on the reduction of the top vapor space. Actually, top vapor space is reduced with respect to the initial value by 40 and 42%, respectively, in the VC and case study "**b**," while in case study "**a**" only by 11%.

Finally, it is worth mentioning that the simulations allowed investigating the behavior of the liquid in the vessel till the PRV opening. After the PRV opening, strong recirculation and mixing phenomena take place, associated to vessel

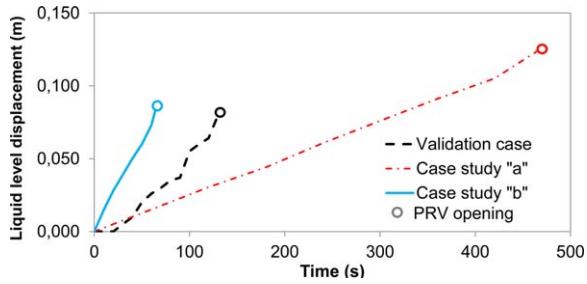

Figure 8. Comparison between the liquid thermal expansion predicted in the VC, case-study "a," and case-study "b." Liquid thermal expansion is reported in terms of liquid level displacement (m).

[Color figure can be viewed in the online issue, which is available at wileyonlinelibrary.com.]

depressurization and to the vent of the fluid through the PRV, as well as to a rapid evaporation of the liquid that leaves the vessel in the gas phase. Hence, both the liquid and the vapor phases feature velocities which may be one or two orders of magnitude higher with respect to those predicted when the PRV is closed and the stratification take places. Thus, the current CFD model is not able to simulate the behavior of the vessel after the PRV opening time. This would require a change in the domain, adding a mass exit as well as an adaptive mesh, which should consider the relevant change in the velocity magnitude and in the thermal boundary layer evolution, which may constitute a further development of the present study.

Conclusions

A CFD model was developed for the assessment of the internal fluid temperature and pressure profile in pressurized vessels containing a liquefied gas under pressure exposed to a fire. The results showed the importance of liquid stratification and liquid thermal expansion on the internal pressure rise of a vessel exposed to external fire. CFD results are particularly important to point out that in the case of high heating loads and high liquid filling levels, the rise of internal pressure is far more influenced by local liquid stratification than by the average liquid temperature raise. Thus, the present model is a first step to include the simulation of the fundamental heat and mass-transfer phenomena occurring in a vessel exposed to fire in the assessment of the time to failure, in the framework of safety and loss prevention aimed at the control of domino effect and escalation hazard.[60–64] In perspective, some simplifications adopted for the development of the model may be dropped. In particular, the assumptions concerning a 2-D domain, considering the vapor as a transparent medium in the calculation of the radiative heat transfer in the top vapor space and imposing a time-averaged incoming heat flux may be removed. However, the main future challenge will be the assessment of the vessel behavior after the opening of the PRV, in which complicating mixing phenomena induced by the fluid motion associated to the discharge may significantly change the nature of the stratified fluid, affecting the behavior of the pressure build-up in the vessel.

Notation

a = droplet volumetric interfacial area, m^{-1}
a_{PR} = first Peng–Robinson equation coefficient
b_{PR} = second Peng–Robinson equation coefficient
$C_{1\varepsilon}$, $C_{2\varepsilon}$, C_μ = standard K-ε turbulence model constants
c_p = specific heat, J/(kg K)
D_{MS} = mean Sauter diameter, m
e = specific energy, J/kg
E_e = contribution to energy balance due to conduction and external source term, J/(m^3 s)
$\mathbf{F}$ = external volumetric force, N/(m^3 s)
F_m = contribution to momentum balance due to gravity and external volumetric forces, kg/(m^2 s^2)
$\mathbf{g}$ = gravity constant, m/s^2
I_ν = incident radiation, W/m^2
$\bar{\bar{\mathbf{I}}}$ = identity tensor
J = evaporation/condensation mass flux, kg/(m^2 s)
K = turbulence kinetic energy, m^2/s^2
k = thermal conductivity, W/(mK)
k_{eff} = effective thermal conductivity, W/(mK)
M = mass source term due to condensation/evaporation phenomena, kg/(m^3 s)
M_w = molar mass, kg/kmol
P = pressure, Pa
Pr = Prandtl number, $\mu/(c_p\ k)$
R = universal gas constant, kJ/(kmol K)
s = ray trace for radiation, m
S = energy source term due to condensation or evaporation, J/(m^3 s)
S_K = turbulence kinetic energy source term, kg/(m s^3)
S_ε = turbulence dissipation rate source term, kg/(m s^4)
t = time, s
T = temperature, K
$T_{L,av}$ = average liquid temperature, K
$\mathbf{u}$ = velocity vector, m/s
$\bar{\mathbf{u}}$ = time averaged two-phase velocity, m/s
$\tilde{\mathbf{u}}$ = time fluctuating two-phase velocity, m/s
v_m = molar volume, m^3/mol
X = mass source term generic expression, kg/(m^3 s)

Greek letters

α = volume fraction of a phase
β = accommodation coefficient for condensation or evaporation
β' = mass-transfer time relaxation parameter, s^{-1}
χ_1 = production/destruction term for turbulence kinetic energy
χ_2 = production/destruction term for turbulence kinetic energy dissipation rate
ε = turbulence kinetic energy dissipation rate, m^2/s^3
η_{abs} = absolute error (see Tables 6 and 7)
η_{rel} = relative error (see Tables 6 and 7)
λ = latent heat of vaporization, J/kg
μ = dynamic viscosity, Pa s
μ_t = turbulent dynamic viscosity, Pa s
Π = dynamic stratification index
ρ = density, kg/m^3
σ_K, σ_ε = standard K-ε turbulence model constants
ξ = mass average two-phase property
ζ = volume fraction average two-phase property
ω = acentric factor
ψ = Peng–Robinson equation parameter (see Table 3)
Ξ = parameter used for model validation (see Tables 7 and 8)

Subscripts

c = critical
cr = data predicted with the "coarse" mesh, for example, the one adopted in the present study
C = condensation
CL = condensation effect on liquid phase
CV = condensation effect on vapour phase
E = evaporation
EL = evaporation effect on liquid phase
EV = evaporation effect on vapour phase
exp = experimental data
fn = data predicted with the "fine" mesh
L = liquid
mod = data predicted by the CFD model
V = vapor
T = turbulence quantity
o = reference quantity

Superscripts

T = transposed
$^\circ$ = saturation condition

Acronyms

BLEVE = boiling liquid expanding vapor explosion
CFD = computational fluid dynamics
LPG = liquefied petroleum gas
PRV = pressure relief valve
S2S = surface to surface radiation model
UDF = user defined function
VOF = volume of fluid method

Literature Cited

1. Van Aerde M, Stewart A, Saccomanno F. Estimating the impacts of L.P.G. spills during transportation accidents. *J Hazard Mater*. 1988; 20:375–392.

2. Paltrinieri N, Bonvicini S, Spadoni G, Cozzani V. Cost-benefit analysis of passive fire protections in road LPG transportation. *Risk Anal*. 2012;32(2):200–219.
3. U.S. Department of Transportation. Lac-Mégantic railroad accident discussion and DOT safety recommendations. Report 4910-06-P. Washington, DC: Department of Transportation, 2013.
4. National Transportation Safety Board. Preliminary report railroad DCA14MR004. Available at http://www.ntsb.gov/doclib/reports/2014/Casselton_ND_Preliminary.pdf. Accessed on July 16, 2014.
5. Landucci G, Tugnoli A, Busini V, Derudi M, Rota R, Cozzani V. The Viareggio LPG accident: lessons learnt. *J Loss Prev Process Ind*. 2011;24(4):466–476.
6. Pontiggia M, Landucci G, Busini V, Derudi M, Alba M, Scaioni M, Bonvicini S, Cozzani V, Rota R. CFD model simulation of LPG dispersion in urban areas. *Atmos Environ*. 2011;45(24):3913–3923.
7. AEA Technology, Major Hazards Assessment Unit. MHIDAS – Major Hazard Incident Data Service. London, UK: Health and Safety Executive, 2003.
8. Reid RC. Possible mechanism for pressurized-liquid tank explosions or BLEVE's. *Science*. 1979;203:1263–1265.
9. Venart JES. Boiling Liquid Expanding Vapor Explosions (BLEVE): possible failure mechanisms. *ASTM Special Technical Publication, Vol. 1336*. 1999:112–134.
10. Roberts AF. The effect of conditions prior to loss of containment on fireball behavior. *The Assessment of Major Hazards*. Rugby, UK: Institute of Chemical Engineers, 1982.
11. Birk AM, Cunningham MH. The boiling liquid expanding vapour explosion. *J Loss Prev Process Ind*. 1994;7(6):474–480.
12. Moodie K. Experiments and modelling: an overview with particular reference to fire engulfment. *J Hazard Mater*. 1988;20:149–175.
13. Birk AM. Hazards from propane BLEVEs: an update and proposal for emergency responders. *J Loss Prev Process Ind*. 1996;9(2):173–181.
14. Han YM, Wang RZ, Dai YJ. Thermal stratification within the water tank. *Renew Sustain Energy Rev*. 2009;13:1014–1026.
15. Gandhi MS, Joshi JB, Vijayan PK. Study of two phase thermal stratification in cylindrical vessels: CFD simulations and PIV measurements. *Chem Eng Sci*. 2013;98:125–151.
16. Cai J, Watanabe T. Numerical simulation of thermal stratification in cold legs by using OpenFOAM. *Prog Nucl Sci Technol*. 2011;2:107–113.
17. Gursu S, Sherif SA, Veziroglu TN, Sheffield JW. Analysis and optimization of thermal stratification and self-pressurization effects in liquid hydrogen storage systems - part 1: model development. *J Energy Resour Technol*. 1993;115(3):221–227.
18. Gursu S, Sherif SA, Veziroglu TN, Sheffield JW. Analysis and optimization of thermal stratification and self-pressurization effects in liquid hydrogen storage systems - part 2: model results and conclusions. *J Energy Resour Technol*. 1993;115(3):228–231.
19. Das SP, Chakraborty S, Dutta P. Studies on thermal stratification phenomenon in LH2 storage vessel. *Heat Transf Eng*. 2004;25(4):54–66.
20. Ren J-J, Shi J-Y, Liu P, Bi M-S, Jia K. Simulation on thermal stratification and de-stratification in liquefied gas tanks. *Int J Hydrogen Energy*. 2013;38(10):4017–4023.
21. Roh S, Son G, Song G, Bae J. Numerical study of transient natural convection in a pressurized LNG storage tank. *Appl Therm Eng*. 2013;52:209–220.
22. Wang L, Li Y, Li C, Zhao Z. CFD investigation of thermal and pressurization performance in LH2 tank during discharge. *Cryogenics*. 2013;57:63–73.
23. Beynon GV, Cowley LT, Small LM, Williams I. Fire engulfment of LPG tanks: HEAT-UP a predictive model. *J Hazard Mater*. 1988;20:227–238.
24. Ramskill PK. A description of the "Engulf" computer code - codes to model the thermal response of an LPG tank either fully or partially engulfed by fire. *J Hazard Mater*. 1988;20:177–196.
25. Ramskill PK. *ENGULF II – A Computer Code to Model the Thermal Response of a Tank Partially or Totally Engulfed in Fire*. Culcheth, UK: Safety and Reliability Directorate [SRD/HSE/R480], 1989.
26. Salzano E, Picozzi B, Vaccaro S, Ciambelli P. Hazard of pressurised tanks involved in fires. *Ind Eng Chem Res*. 2003;42:1804–1812.
27. Lautkaski R. Evaluation of BLEVE risks of tank wagons carrying flammable liquids. *J Loss Prev Process Ind*. 2009;22:117–123.
28. Landucci G, Gubinelli G, Antonioni G, Cozzani V. The assessment of the damage probability of storage tanks in domino events. *Accident Anal Prev*. 2009;41(6):1206–1215.
29. Aydemir NU, Magapu VK, Sousa ACM, Venart JES. Thermal response analysis of LPG tanks exposed to fire. *J Hazard Mater*. 1988;20:239–262.
30. Birk AM. Modelling the effects of a torch-type fire impingement on a rail or highway tanker. *Fire Saf J*. 1989;15:277–296.
31. Dancer D, Sallet DW. Pressure and temperature response of liquefied gases in containers and pressure vessels which are subjected to accidental heat input. *J Hazard Mater*. 1990;25:3–18.
32. Gong YW, Lin WS, Gu AZ, Lu XS. A simplified model to predict the thermal response of PLG and its influence on BLEVE. *J Hazard Mater*. 2004;A108:21–26.
33. Shi J, Ren J, Liu P, Bi M. Experimental research on the effects of fluid and heater on thermal stratification of liquefied gas. *Exp Therm Fluid Sci*. 2013;50:29–36.
34. Birk AM. Scale effects with fire exposure of pressure-liquefied gas tanks. *J Loss Prev Process Ind*. 1995;8(5):275–290.
35. Yu CM, Aydemir NU, Venart JES. Transient free convection and thermal stratification in uniformly-heated partially-filled horizontal cylindrical and spherical vessels. *J Therm Sci*. 1992;1(2):114–122.
36. Birk AM, Cunningham MH. Liquid temperature stratification and its effect on BLEVEs and their hazards. *J Hazard Mater*. 1996;48:219–237.
37. Hadjisophocleousl GV, Souse ACM, Venart JES. A study of the effect of the tank diameter on the thermal stratification of LPG vessel subjected to fire engulfment. *J Hazard Mater*. 1990;25:19–31.
38. Bi M-S, Ren J-J, Zhao B, Che W. Effect of fire engulfment on thermal response of LPG tanks. *J Hazard Mater*. 2011;192:874–879.
39. Townsend W, Anderson CE, Zook J, Cowgill G. Comparison of thermally coated and uninsulated rail tank-cars filled with LPG subjected to a fire environment. Report FRA-OR&D 75-32. Washington, DC: US Department of Transportation, 1974.
40. ANSYS, Inc. *ANSYS® FLUENT® 14.5 Theory Guide*. Cecil Township, PA: ANSYS, Inc., 2012.
41. Tu J, Yeoh G, Liu C. *Computational Fluid Dynamics. A Practical Approach*, 2nd ed. Waltham, MA: Butterworth-Heinemann, 2013.
42. Andersson B, Andersson R, Håkansson L, Mortensen M, Sudiyo R, van Wachem B. *Computational Fluid Dynamics for Engineers*. Cambridge, UK: Cambridge University Press, 2012.
43. Hirt CW, Nichols BD. Volume of fluid (VOF) method for the dynamics of free boundaries. *J Comput Phys*. 1981;39(1):201–225.
44. Hiroharu K, Niichi N, Masaru H. On the turbulent heat transfer by free convection from a vertical plate. *Int J Heat Mass Transf*. 1968;11(7):1117–1125.
45. Launder BE, Spalding DB. *Lectures in Mathematical Models of Turbulence*. London, UK: Academic Press, 1972.
46. Youngs DL. Time-dependent multi-material flow with large fluid distortion. In: Morton KW, Baines MJ, editors. *Numerical Methods for Fluid Dynamics*. London, UK: Academic Press, 1982:273–285.
47. Reddy KS, Kumar NS. Combined laminar natural convection and surface radiation heat transfer in a modified cavity receiver of solar parabolic dish. *Int J Therm Sci*. 2008;47:1647–1657.
48. Lu X, Wang T. Investigation of radiation models in entrained-flow coal gasification simulation. *Int J Heat Mass Transf*. 2013;67:377–392.
49. Knudsen M. *The Kinetic Theory of Gases: Some Modern Aspects*. London: Methuen and Co., Ltd, 1934.
50. Smith JM, Van Ness HC, Abbott MM. *Introduction to Chemical Engineering Thermodynamics*, 7th ed. New York, NY: McGraw-Hill, 2005.
51. Crowe CT, Schwarzkopf JD, Sommerfeld M, Tsuji Y. *Multiphase Flows with Droplets and Particles*, 2nd ed. Boca Raton, FL: CRC Press, Taylor and Francis Group, 2012.
52. Wu HL, Peng XF, Ye P, Eric Gong Y. Simulation of refrigerant flow boiling in serpentine tubes. *Int J Heat Mass Transf*. 2007;50(5–6):1186–1195.
53. American Society for Testing and Materials. *ASTM D1835-13 Standard Specification for Liquefied Petroleum (LP) Gases*. West Conshohocken, PA: ASTM International, 2014.
54. Liley PE, Thomson GH, Friend DG, Daubert TE, Buck E. Physical and chemical data. In: Perry RH, Green DW, editors. *Perry's Chemical Engineers' Handbook*, 7th ed. New York: McGraw-Hill, 1999.

55. Launder BE, Spalding DB. The numerical computation of turbulent flows. *Comput Methods Appl Mech Eng*. 1974;3(2):269–289.
56. National Archives and Records Administration. *Code of Federal Regulations Title 49, Transportation, Parts 178–199 2013*. Baton Rouge, LA: Claitor's Publishing Division, Incorporated, 2013.
57. Birk AM. Scale effects with fire exposure of pressure-liquefied gas tanks. *J Loss Prev Process Ind*. 1995;8(5):275–290.
58. Moodie K, Cowley LT, Denny RB, Small LM, Williams I. Fire engulfment tests on a 5 tonne LPG tank. *J Hazard Mater*. 1988;20:55–71.
59. Landucci G, Cozzani V, Birk AM. Heat radiation effects. In: Cozzani V, Reniers G, editors. *Domino Effects in the Process Industries. Modelling, Prevention and Managing*. Amsterdam: Elsevier, 2013:70–115.
60. Manu CC, Birk AM, Kim IY. Stress rupture predictions of pressure vessels exposed to fully engulfing and local impingement accidental fire heat loads. *Eng Fail Anal*. 2009;16:1141–1152.
61. Birk AM. Scale considerations for fire testing of pressure vessels used for dangerous goods transportation. *J Loss Prev Process Ind*. 2012;25:623–630.
62. Landucci G, Molag M, Cozzani V. Modeling the performance of coated LPG tanks engulfed in fires. *J Hazard Mater*. 2009;172(1):447–456.
63. Landucci G, Molag M, Reinders J, Cozzani V. Experimental and analytical investigation of thermal coating effectiveness for 3 m^3 LPG tanks engulfed by fire. *J Hazard Mater*. 2009;161(2–3):1182–1192.
64. Paltrinieri N, Landucci G, Molag M, Bonvicini S, Spadoni G, Cozzani V. Risk reduction in road and rail LPG transportation by passive fire protection. *J Hazard Mater*. 2009;167(1–3):332–344.

Manuscript received Apr. 23, 2014, and revision received July 18, 2014.